ISA Transactions 165 (2025) 64–71

Contents lists available at ScienceDirect

ISA Transactions

journal homepage: www.elsevier.com/locate/isatra

Research article

Memory-based dynamic event-triggered secure control of active suspension systems against deception attacks☆

Wangrui Cheng[a], Tingting Yin[b], Zhou Gu[b,*]

[a] School of Mathematics-Physics and Finance, Anhui Polytechnic University, Wuhu 241000, China
[b] School of Electrical Engineering, Anhui Polytechnic University, Wuhu 241000, China

HIGHLIGHTS

- A novel memory-based dynamic event-triggered mechanism is introduced, integrating past release information and a dynamic parameter updating law to optimize resource utilization under deception attacks.
- The proposed mechanism leverages historical triggering data and errors, improving adaptability to random attacks and unexpected disturbances while facilitating efficient network data transmission.
- The control strategy enhances driving comfort and safety by ensuring mean square asymptotic stability and H_∞ control performance, validated through Carsim and Matlab simulations.

ARTICLE INFO

Keywords:
Memory-based dynamic ETM
Deception attacks
Quarter-vehicle suspension systems

ABSTRACT

This study deals with the issue of a memory-based dynamic event-triggered control strategy for active quarter-vehicle suspension systems (QVSSs). The main objective is to design an effective event-triggered mechanism (ETM) that ensures suspension performance while reducing network resource usage, even under deception attacks. To this end, an innovative memory-based dynamic ETM is proposed to coordinate sensor data transmission efficiently in the presence of such attacks. The proposed transmission scheme integrates historical release information, which helps suppress false triggering by utilizing averaged data. Additionally, the proposed ETM dynamically updates triggering conditions over time, facilitating dynamic scheduling of network data transmission. Sufficient conditions are derived to guarantee satisfactory performance of the QVSS under the proposed control strategy. A numerical example is provided to validate the effectiveness of the approach.

1. Introduction

Vehicle suspension systems (SSs) have gained significant attention over the past few decades due to their crucial role in ensuring both driving comfort and safety [1–3]. The development of vehicle SSs typically targets three key performance criteria: ride comfort, suspension stroke, and road holding. Ride comfort is primarily associated with the vertical acceleration of the vehicle body in response to road irregularities. Road holding refers to the suspension system's ability to maintain consistent and secure contact between the tires and the road surface. Suspension stroke denotes the allowable range of motion for the vehicle chassis. However, these requirements often conflict with one another, necessitating the use of advanced suspension designs and intelligent control strategies to achieve an optimal balance under complex driving conditions [4].

SS are generally classified into passive, semi-active, and active types, each of which differs according to the inclusion of controllable components. Passive SSs, which lack such components, typically consist of a fixed spring and a damper with a constant damping coefficient. While simple and reliable, they are inadequate for meeting the conflicting performance requirements of ride comfort, suspension stroke, and road holding. Semi-active SSs offer a compromise by integrating controllable damping components that continuously adjust the energy

☆ This work was supported by the National Natural Science Foundation of China under Grant 62273183, and in part by the Natural Science Foundation of Jiangsu Province of China under Grant BK20231288, and in part the Startup Funding of Anhui Polytechnic University under Grant 2024YQQ001.

* Corresponding author.
Email addresses: 2241021108@stu.ahpu.edu.cn (W. Cheng), yintingting@stu.ahpu.edu.cn (T. Yin), guzhou@stu.ahpu.edu.cn (Z. Gu).

https://doi.org/10.1016/j.isatra.2025.06.007
Received 2 March 2025; Received in revised form 22 May 2025; Accepted 6 June 2025
Available online 17 June 2025

dissipation rate, thereby enhancing comfort and road contact. However, their performance is limited by the absence of external actuation forces and a narrow effective frequency range. In contrast, active SSs employ fast-response actuators to dynamically generate vertical forces in real time, significantly improving handling performance across various road and load conditions. Due to fewer physical constraints and a flexible structure, active SSs are widely regarded as superior to both passive and semi-active systems, particularly owing to their use of linear force actuators [5,6]. As a result, numerous control strategies have been developed for actuator regulation in active SSs, including fuzzy control [7–9], sliding-mode control [10,11], and backstepping control [12,13], among others.

The rapid advancement of communication technologies has led to the emergence of networked SS. This evolution introduces new challenges for traditional control strategies. In [14], a resilient event-triggered H_∞ controller was designed for QVSSs under periodic denial-of-service (DoS) attacks. Similarly, an event-based fuzzy controller was proposed for networked five-degree-of-freedom semi-vehicle SSs in [15], addressing the impact of DoS attacks on wireless networks. To cope with the nonlinearities and uncertainties inherent in cloud-aided full-vehicle SSs, an adaptive backstepping control approach was developed in [13]. Notably, the controller in [13] leverages a cloud-based master computing server, which considers multiple factors including aggregated vehicle data, road conditions, and reference trajectories stored in the cloud.

A critical challenge in the research of networked SSs lies in the limitation of network bandwidth. This issue becomes particularly prominent in networked control systems. ETMs have gained significant attention as an effective solution to this challenge [16–20]. In [21], sampled data packets are selectively transmitted over the network only when a predefined triggering condition is satisfied, allowing for more efficient bandwidth usage and substantial savings. To further reduce redundant data transmission between sensors and controllers and to mitigate the adverse effects of asynchronous switching and denial-of-service (DoS) attacks, a resilient adaptive event-triggered strategy was proposed for networked switched systems in [22]. ETMs have also been applied to various control problems in networked SSs, including event-triggered reliable finite-frequency control [23], event-triggered adaptive fixed-time fuzzy control [24], and memory-event-trigger-based secure control [25]. As research in this area has advanced, several innovative ETMs have emerged, such as memory-based ETMs [26], adaptive ETMs [27], and dynamic ETMs [28,29]. Nevertheless, the application of these advanced ETM strategies to networked SSs has received limited attention, thereby serving as a key motivation for this study.

Since the data received by the controller is transmitted via the network, ensuring the reliability and security of this information is crucial—particularly in the face of cyber-attacks targeting the network infrastructure [30–32]. Among various attack strategies, deception attacks are especially concerning. This type of attack typically involves the interception and manipulation of transmitted information, leading remote nodes to process false or misleading data. Deceptive signals often infiltrate multiple communication channels, making them highly covert and difficult to detect. In [33], a dynamic output feedback controller was proposed to counter deception attacks in discrete-time stochastic nonlinear systems. A more comprehensive scenario was studied in [34], where deception attacks affect both sensor–observer and controller–actuator communication paths, with a variety of deceptive signals launched in a stochastic manner. Such attacks pose a significant threat to the performance and stability of networked SSs. Therefore, it is imperative to thoroughly investigate the resilience and behavior of networked SSs under deception attacks, which constitutes another key motivation for this study.

Motivated by the above discussion, this paper investigates the problem of memory-based dynamic event-triggered control for active SSs under deception attacks. The main contributions of this work are summarized as follows:

(1) This paper proposes a novel memory-based dynamic ETM to ensure the performance of active QVSSs while reducing resource utilization under deception attacks. The proposed ETM utilizes past release information as input, thereby reducing false-triggered events by incorporating average historical data. In contrast to the memory-based ETMs presented in [20,26], this work introduces a new dynamic parameter updating law. Moreover, historical triggering data are embedded within the updating law, which significantly enhances the dynamic scheduling of network data transmission. In addition, the event-triggering condition incorporates historical error information, improving sensitivity to random attacks and unexpected disturbances.

(2) The proposed memory-based dynamic ETM enhances both driving comfort and safety for active QVSSs operating under deception attacks. The control strategy effectively optimizes the data transmission workload and transmitted information, while ensuring mean square asymptotic stability and achieving desired H_∞ control performance. Simulation results validate the effectiveness of the proposed protocol in meeting the dual objectives of driving safety and ride comfort.

The subsequent sections of this paper present a summary of its contents. In Section 2, we provide the problem formulation. The controller design for networked active QVSSs against deception attacks is expounded in Section 3. To demonstrate the effectiveness of our method, a simulation example is presented in Section 4. Finally, we conclude the paper with a summary in Section 5.

2. Problem formulation

2.1. System description and performance indices

The following active QVSS structure [8] is widely adopted for its ability to capture the essential characteristics of suspension systems.

$$\begin{cases} \dot{x}(t) = Ax(t) + Bu(t) + D\omega(t) \\ z_1(t) = C_1 x(t) + D_1 u(t) \\ z_2(t) = C_2 x(t) \end{cases} \tag{1}$$

where

$$x(t) = \begin{bmatrix} x_1^T(t) & x_2^T(t) & x_3^T(t) & x_4^T(t) \end{bmatrix}^T,$$

$$A = \begin{bmatrix} 0 & 0 & 1 & -1 \\ 0 & 0 & 0 & 1 \\ -\frac{k_s}{m_s} & 0 & -\frac{c_s}{m_s} & \frac{c_s}{m_s} \\ \frac{k_s}{m_u} & -\frac{k_t}{m_u} & \frac{c_s}{m_u} & -\frac{c_s + c_t}{m_u} \end{bmatrix}, B = \begin{bmatrix} 0 & 0 & \frac{1}{m_s} & -\frac{1}{m_u} \end{bmatrix}^T,$$

$$C_1 = \begin{bmatrix} -\frac{k_s}{m_s} & 0 & -\frac{c_s}{m_s} & \frac{c_s}{m_s} \end{bmatrix}, C_2 = \begin{bmatrix} \frac{1}{z_{max}} & 0 & 0 & 0 \\ 0 & \frac{k_t}{(m_u + m_s)g} & 0 & 0 \end{bmatrix},$$

$$D = \begin{bmatrix} 0 & -1 & 0 & \frac{c_t}{m_u} \end{bmatrix}^T, D_1 = \frac{1}{m_s}.$$

The terminologies of the SS refer to [15].

2.2. Performance indices

Drawing parallels with the work of [15], the following critical indices considering ride comfort, suspension deflection, and road holding are presented, as elaborated in Table 1.

In Table 1, the quantity $\ddot{z}_s(t)$ appearing in index (i) corresponds to the body acceleration, illustrating the dynamic response of the system. The second index and the third index pertain to the analysis of the mechanical structure's stroke and the assessment of driving stability, respectively. The parameter z_{max} represents the prescribed admissible stroke of the mechanical structure, $(m_u + m_s)g$ denotes the static load, and g symbolizes the gravity acceleration.

Table 1
Critical indices of the QVSS.

	Performance	Indicator
(i)	Ride comfort	$\mathbb{E}\left\{ \parallel \ddot{z}_s(t) \parallel_2 \right\} < \gamma^2 \mathbb{E}\left\{ \parallel \omega(t) \parallel_2 \right\}$
(ii)	Suspension stroke	$\mathbb{E}\left\{ \mid z_s(t) - z_u(t) \mid \right\} \leq z_{max}$
(iii)	Road holding	$\mathbb{E}\left\{ k_t(\mid z_u(t) - z_r(t)) \mid \right\} \leq (m_u + m_s)g$

2.3. Communication strategy

Notice that the control data of SSs, communicated through the wireless network, can lead to challenges related to limited network resources and vulnerabilities to deception attacks. Here, we present a new memory-based dynamic ETM to alleviate the strain on communication resources and enhance resilience against deception attacks.

2.3.1. Memory-based dynamic ETM

Before proposing the memory-based dynamic ETM to address the aforementioned challenge, we define

$$\begin{aligned}
&\bar{x}(t_{k-m+1}h) = \frac{x(t_{k-m+1}h) + x(t_k h + lh)}{2},\ m \in \{1,2,3\},\\
&e_m(t) = x(t_{k-m+1}h) - \bar{x}(t_{k-m+1}h),\\
&\vartheta_1(t) = \frac{1}{3}\sum_{m=1}^{3} x(t_{k-m+1}h),\\
&\vartheta_{e1}(t) = e_2(t) - e_1(t), \vartheta_{e2}(t) = e_3(t) - e_2(t)\\
&\vartheta(t) = \delta_1 \vartheta_1^T(t)\Phi\vartheta_1(t) + \delta_2(\vartheta_{e1}^T(t)\Phi\vartheta_{e2}(t) + \vartheta_{e2}^T(t)\Phi\vartheta_{e1}(t)),\\
&\psi(t) = \sum_{m=1}^{3} \lambda_m e_m^T(t)\Phi e_m(t) - \vartheta(t)
\end{aligned} \tag{2}$$

where h represents the sampling period, and $\{t_k h\}_{k=0}^{\infty}$ denotes the monotonically increasing sequence of release instants. The parameters δ_1, δ_2, and λ_m are predetermined weighting scalars, while Φ corresponds to the weighting matrix.

Subsequently, the next release instant can be defined by

$$t_{k+1}h = t_k h + \max\left\{(l+1)h \mid \psi(t) < \frac{1}{\kappa}\beta(t)\right\} \tag{3}$$

where $\dot{\beta}(t) = -a\beta(t) - \sigma\psi(t)$ for $t \in [t_k h, t_{k+1}h)$, with $a > \frac{1}{\kappa} > 0$, $\sigma > 0$, and $\beta(0) = \beta_0 \geq 0$. It implies that when designed condition $\psi(t) < \frac{1}{\kappa}\beta(t)$ is violated, the packet at such sampling instant becomes necessary for controlling the SS, but the packets at times $t_k h + lh$ are disregarded, where $l = 1, 2, \ldots, l_M \triangleq \max_{\kappa\psi(t)<\beta(t)} l$, for $t \in [t_k h, t_{k+1}h)$.

Remark 1. From (2), it is evident that the historical triggering data $x(t_{k-m+1}h)$, where $m \in 1,2,3$, are incorporated into the ETM design, offering several notable advantages: it helps mitigate false-triggering events caused by sudden and unintended state variations, such as gross measurement errors; furthermore, it facilitates a smoother and more gradual release process.

Remark 2. Incorporating additional historical packets into the ETM input increases storage and computational demands. To balance computational cost and performance, the number of historical triggering data packets is limited to three in this study, i.e., $\bar{m} = 3$, and $m \in 1,2,3$.

Remark 3. The item $\delta_2(\vartheta_{e1}^T(t)\Phi\vartheta_{e2}(t) + \vartheta_{e2}^T(t)\Phi\vartheta_{e1}(t))$ in (3) uses the error of historical triggering information, which can enhance the sensibility to random attacks and unknown disturbances.

Remark 4. The proposed memory-based dynamic ETM mainly comprises two main components: a memory-based event triggering law and a dynamic parameter updating law. By incorporating $\beta(t)$ in (5), system designers are granted the flexibility to specify positive constants a, κ, σ as desired. This empowers them to schedule the transmission rate over specific time intervals, reducing network resource waste.

2.3.2. State feedback secure control

In light of the presented memory-based dynamic ETM in (3), the state feedback control law is given:

$$\bar{u}(t) = \sum_{m=1}^{3} K_m x(t_{k-m+1}h), t \in [t_k h + \eta_k, t_{k+1}h + \eta_{k+1}) \tag{4}$$

where η_k is the network-induce delay at instant $t_k h$.

Considering the potential influence of attacks on the transmitted signal, we establish the following model to represent the data received by the controller:

$$\tilde{x}(t_{k-m+1}h) = \alpha(t_{k-m+1}h)\aleph(t_{k-m+1}h) + (1 - \alpha(t_{k-m+1}h))x(t_{k-m+1}h) \tag{5}$$

Remark 5. The control signal becomes susceptible to potential attacks upon its transmission through the network. Adversarial elements exploit this vulnerability by surreptitiously injecting spurious data denoted as $\aleph(t)$ into the transmitting signal. In order to elude detection, the attack signal is meticulously generated in a stochastic manner, concurrently with the intentional omission of certain transmitted signals. $\aleph(t)$ is assumed to satisfy [26]

$$||\aleph(t)||_2 \leq ||Lx(t)||_2. \tag{6}$$

Consequently, the actual control input can be formulated as:

$$u(t) = \sum_{m=1}^{3}(1 - \alpha(t_{k-m+1}h))K_m x(t_{k-m+1}h) + \sum_{m=1}^{3}\alpha(t_{k-m+1}h)K_m\aleph(t_{k-m+1}h) \tag{7}$$

in which $\alpha(t)$ means a stochastic variable that adheres to a Gaussian distribution with mean $\bar{\alpha}$ and variance $\hat{\alpha}$.

2.4. The closed-loop quarter-vehicle suspension control system

Define $\eta(t) = t - t_k h - lh$ for $t \in [t_k h + lh + \eta_k^l, t_{k+1}h + lh + h + \eta^{l+1}k + 1)$. Consequently, the following inequality is obtained:

$$0 \leq \eta(t) \leq h + \bar{\eta} = \eta_M. \tag{8}$$

From (2) and (8), we can deduce that:

$$x(t_{k-m+1}h) = x(t - \eta(t)) + 2e_m(t). \tag{9}$$

Combining Eqs. (1), (7), and (9), we can derive the closed-loop active QVSS model as

$$\begin{cases}
\dot{x}(t) = \sum_{m=1}^{3}\Big[Ax(t) + (1 - \alpha(t_{k-m+1}))BK_m x(t - \eta(t))\\
\qquad + (1 - \alpha(t_{k-m+1}))2BK_m e_m(t)\\
\qquad + \alpha(t_{k-m+1}h)BK_m\aleph(t_{k-m+1}h) + D\omega(t)\Big]\\
z_1(t) = \sum_{m=1}^{3}\Big[C_1 x(t) + (1 - \alpha(t_{k-m+1}))D_1 K_m x(t - \eta(t))\\
\qquad + (1 - \alpha(t_{k-m+1}))2D_1 K_m e_m(t)\\
\qquad + \alpha(t_{k-m+1}h)D_1 K_m\aleph(t_{k-m+1}h)\Big]\\
z_2(t) = C_2 x(t).
\end{cases} \tag{10}$$

Next, we will design the suspension control based on the above memory-based dynamic ETM for the active QVSS in (10) against deception attacks.

3. Memory-based dynamic ETM for QVSSs

In this section, we will obtain sufficient conditions to ensure the control performance of active QVSSs under memory-based dynamic ETM against deception attacks.

Theorem 1. *Given positive scalars λ_m, η_M, $\bar{\alpha}$, $\hat{\alpha}$, a, κ, σ, and δ_i ($i \in 1,2$), as well as the matrix K_m ($m \in \{1,2,3\}$), the system (10) is mean square asymptotically stable (MSAS) and satisfies the H_∞ performance indices listed in Table 1, if there exist matrices $P>0$, $Q>0$, $R>0$, and $\Phi>0$ such that*

$$\Psi < 0, \tag{11}$$

$$\begin{bmatrix} -I & * \\ \sqrt{\nu}\{C_2\}_n^T & -P \end{bmatrix} < 0, \ (n=1,2) \tag{12}$$

$$\mathcal{R} > 0 \tag{13}$$

where

$$\Psi = \Psi_1 + \Psi_2, \Psi_1 = [\Pi]_{12\times 12}, \Pi_{11} = A^T P + PA + Q - 4R,$$
$$\Pi_{21} = \sum_{m=1}^{3}(1-\bar{\alpha})(K_m^T B^T P) - 2R - H_1^T - H_2 - H_2^T - H_3^T,$$
$$\Pi_{22} = \mu_1\Phi - 8R + H_1^T + H_1 - H_3^T - H_3,$$
$$\Pi_{31} = H_1^T - H_2 + H_2^T - H_3^T, \Pi_{33} = -Q - 4R,$$
$$\Pi_{32} = -2R - H_1^T + H_2 + H_2^T - H_3^T,$$
$$\Pi_{(m+3)1} = 2(1-\bar{\alpha})K_m^T B^T P, \Pi_{(m+3)2} = \frac{2}{3}\mu_1\Phi,$$
$$\Pi_{44} = \left(-\mu_{31} + \frac{4}{9}\mu_1\right)\Phi, \Pi_{54} = \left(\frac{4}{9}\mu_1 + \mu_2\right)\Phi,$$
$$\Pi_{55} = \left(-\mu_{32} + \frac{4}{9}\mu_1 - 2\mu_2\right)\Phi, \Pi_{64} = \left(\frac{4}{9}\mu_1 - \mu_2\right)\sigma_4\Phi,$$
$$\Pi_{65} = \left(\frac{4}{9}\mu_1 + \mu_2\right)\Phi, \Pi_{66} = \left(-\mu_{33} + \frac{4}{9}\mu_1\right)\Phi, \Pi_{71} = 6R,$$
$$\Pi_{72} = 6R + 2H_2 + 2H_3, \Pi_{73} = -2H_2 + 2H_3,$$
$$\Pi_{77} = \Pi_{88} = -12R, \Pi_{81} = 2H_2 + H_3^T, \Pi_{83} = 6R,$$
$$\Pi_{82} = 6R - 2H_2 + 2H_3^T, \Pi_{87} = -4H_3^T, \Pi_{1212} = -\gamma^2 I,$$
$$\Pi_{(m+8)1} = \bar{\alpha}K_m^T B^T P, \Pi_{(m+8)(m+8)} = -P, \Pi_{121} = D^T P,$$
$$\mu_1 = (1+\sigma)\delta_1, \mu_2 = (1+\sigma)\delta_2, \mu_{3m} = (1+\sigma)\lambda_m,$$
$$\Psi_2 = \eta_M^2 \mathcal{A}^T R\mathcal{A} + \eta_M^2 \mathcal{B}^T R\mathcal{B} + C^T C + \mathcal{D}^T P\mathcal{D},$$
$$\mathcal{A} = \begin{bmatrix} A & (1-\bar{\alpha})\mathscr{B}_1 & 0 & 2(1-\bar{\alpha})\mathscr{B}_2 & 0 & 0 & \bar{\alpha}\mathscr{B}_2 & D \end{bmatrix},$$
$$\mathcal{B} = \begin{bmatrix} 0 & \hat{\alpha}\mathscr{B}_1 & 0 & 2\hat{\alpha}\mathscr{B}_2 & 0 & 0 & \hat{\alpha}\mathscr{B}_2 & 0 \end{bmatrix},$$
$$C = \begin{bmatrix} C_1 & (1-\bar{\alpha})\mathscr{D}_1 & 0 & 2(1-\bar{\alpha})\mathscr{D}_2 & 0 & 0 & \bar{\alpha}\mathscr{D}_2 & 0 \end{bmatrix},$$
$$\mathcal{D} = \begin{bmatrix} \sqrt{3}L & \underbrace{0 \ \dots \ 0}_{11} \end{bmatrix}, H = \begin{bmatrix} H_1 & * \\ H_2 & H_3 \end{bmatrix}, \hat{R} = \begin{bmatrix} R & 0 \\ 0 & 3R \end{bmatrix},$$
$$\mathscr{B}_1 = \sum_{m=1}^{3} BK_m, \mathscr{B}_2 = \begin{bmatrix} BK_1 & BK_2 & BK_3 \end{bmatrix}, \mathcal{R} = \begin{bmatrix} \hat{R} & * \\ H^T & \hat{R} \end{bmatrix},$$
$$\mathscr{D}_1 = \sum_{m=1}^{3} D_1 K_m, \mathscr{D}_2 = \begin{bmatrix} D_1K_1 & D_1K_2 & D_1K_3 \end{bmatrix}.$$

Proof. Construct the following Lyapunov–Krasovskii functional:

$$V(t) = x^T(t)Px(t) + \int_{t-\eta_M}^{t} x^T(s)Qx(s)ds + \eta_M \int_{t-\eta_M}^{t}\int_{s}^{t} \dot{x}^T(v)R\dot{x}(v)dvds + \beta(t). \tag{14}$$

Then, we have

$$\mathbb{E}\{\dot{V}(t)\} \le \mathbb{E}\Big\{ 2x^T(t)P\dot{x}(t) + x^T(t)Qx(t) - x^T(t-\eta_M)Qx(t-\eta_M) + \eta_M^2\dot{x}^T(t)R\dot{x}(t) - \eta_M\int_{t-\eta_M}^{t}\dot{x}^T(s)R\dot{x}(s)ds + \dot{\beta}(t)\Big\}. \tag{15}$$

Drawing upon the triggering condition in (2) and considering the constraints of deception attacks in (6), we can deduce that

$$\begin{aligned}\mathbb{E}\{\dot{V}(t)\} \le \mathbb{E}\Big\{ & 2x^T(t)P\dot{x}(t) + x^T(t)Qx(t) - x^T(t-\eta_M)Qx(t-\eta_M) \\ & + \eta_M^2\dot{x}^T(t)R\dot{x}(t) - \eta_M\int_{t-\eta_M}^{t}\dot{x}^T(s)R\dot{x}(s)ds \\ & - \sum_{m=1}^{3}\left[f^T(t_{k-m+1}h)P\aleph(t_{k-m+1}h) - 3x^T(t)L^T PLx(t)\right] \\ & + \left(\frac{1}{\kappa} - a\right)\beta(t) - \sigma\psi(t) - \psi(t) + z_1^T(t)z_1(t) - \gamma^2\omega^T(t)\omega(t)\Big\}.\end{aligned} \tag{16}$$

For the sake of clarity and brevity, we define

$$\zeta(t) = col\{\zeta_1(t), \zeta_e(t), \zeta_{w1}(t), \zeta_{w2}(t), \zeta_\aleph(t), \omega(t)\}, \Omega_i = T_i\zeta(t), (i=1,2,3,4),$$
$$\hat{\Omega}_1 = col\{\Omega_1, \Omega_2\}, \hat{\Omega}_2 = col\{\Omega_3, \Omega_4\},$$
$$T_1 = [I \ -I \ \underbrace{0 \ \cdots \ 0}_{10}], T_2 = [I \ I \ \underbrace{0 \ \dots \ 0}_{4} \ -2I \ \underbrace{0 \ \cdots \ 0}_{5}],$$
$$T_3 = [0 \ I \ -I \ \underbrace{0 \ \cdots \ 0}_{9}], T_4 = [0 \ I \ I \ \underbrace{0 \ \cdots \ 0}_{4} \ -2I \ \underbrace{0 \ \dots \ 0}_{4}]$$

with $\zeta_1(t) = col\{x(t), x(t-\eta(t)), x(t-\eta_M)\}$, $\zeta_e(t) = col\{e_1(t), e_2(t), e_3(t)\}$, $\zeta_{w1}(t) = \frac{1}{\eta(t)}\int_{t-\eta(t)}^{t} x(s)ds$, $\zeta_{w2}(t) = \frac{1}{\eta_M-\eta(t)}\int_{t-\eta_M}^{t-\eta(t)} x(s)ds$, $\zeta_\aleph(t) = col\{\aleph(t_k h), \aleph(t_{k-1}h), \aleph(t_{k-2}h)\}$.

In light of the characteristics of α, it yields that

$$\mathbb{E}\{\dot{x}^T(t)R\dot{x}(t)\} = \zeta^T(t)(\mathcal{A}^T R\mathcal{A} + \mathcal{B}^T R\mathcal{B})\zeta(t). \tag{17}$$

Using the Wirtinger inequality in [35], one can obtain

$$-\eta_M\int_{t-\eta(t)}^{t}\dot{x}^T(s)R\dot{x}(s)ds \le -\frac{\eta_M}{\eta(t)}\hat{\Omega}_1^T\hat{R}\hat{\Omega}_1, \tag{18}$$

$$-\eta_M\int_{t-\eta_M}^{t-\eta(t)}\dot{x}^T(s)R\dot{x}(s)ds \le -\frac{\eta_M}{\eta_M-\eta(t)}\hat{\Omega}_2^T\hat{R}\hat{\Omega}_2 \tag{19}$$

where $\hat{R} = diag\{R, 3R\}$.

Wirtinger inequality methods [36] to (18) and (19), it can be inferred that

$$\begin{aligned} & -\eta_M\int_{t-\eta_M}^{t}\dot{x}^T(s)R\dot{x}(s)ds \\ & = -\eta_M\int_{t-\eta(t)}^{t}\dot{x}^T(s)R\dot{x}(s)ds - \eta_M\int_{t-\eta_M}^{t-\eta(t)}\dot{x}^T(s)R\dot{x}(s)ds \\ & \le -\begin{bmatrix}\hat{\Omega}_1 \\ \hat{\Omega}_2\end{bmatrix}^T\begin{bmatrix}\frac{\eta_M}{\eta(t)}\hat{R} & 0 \\ 0 & \frac{\eta_M}{\eta_M-\eta(t)}\hat{R}\end{bmatrix}\begin{bmatrix}\hat{\Omega}_1 \\ \hat{\Omega}_2\end{bmatrix} \\ & \le -\begin{bmatrix}\hat{\Omega}_1 \\ \hat{\Omega}_2\end{bmatrix}^T\mathcal{R}\begin{bmatrix}\hat{\Omega}_1 \\ \hat{\Omega}_2\end{bmatrix}\end{aligned} \tag{20}$$

From (16), (17) and (20), it results in

$$\mathbb{E}\left\{\dot{V}(t)\right\} \le \mathbb{E}\left\{\zeta^T(t)\Pi\zeta(t)\right\}. \tag{21}$$

Then, (11) and (13) guarantee that

$$\mathbb{E}\{\dot{V}(t) + z_1^T(t)z_1(t) - \gamma^2\omega^T(t)\omega(t)\} < 0 \tag{22}$$

Define $\nu = \inf\{V(0) + \int_0^t [z_1^T(t)z_1(t) - \gamma^2\omega^T(t)\omega(t)]dt\}$ with $t > 0$. Combining (14) and (22) yields that

$$x^T(t)Px(t) \le \nu. \tag{23}$$

To satisfy the indices (ii) and (iii) depicted in Table 1, it is imperative that the following condition be met:

$$|\{z_2(t)\}_n| \le I \ (n \in \{1,2\}), \tag{24}$$

where $z_2(t)_n$ signifies the n-th row of $z_2(t)$.

From (23), we have

$$\begin{aligned} x^T(t)\{C_2\}_n^T\{C_2\}_n x(t) &= x^T(t)P^{\frac{1}{2}}P^{-\frac{1}{2}}\{C_2\}_n^T\{C_2\}_n P^{-\frac{1}{2}}P^{\frac{1}{2}}x(t) \\ &\le \lambda_{\max}\left\{P^{-\frac{1}{2}}\{C_2\}_n^T\{C_2\}_n P^{-\frac{1}{2}}\right\}x^T(t)Px(t) \\ &\le \lambda_{\max}\left\{\nu P^{-\frac{1}{2}}\{C_2\}_n^T\{C_2\}_n P^{-\frac{1}{2}}\right\} \end{aligned} \tag{25}$$

where $\{C_2\}_n$ denotes the n-th row of C_2.

Applying Schur complement to (12) results in the following:

$$\nu P_g^{-\frac{1}{2}}\{C_2\}_n^T\{C_2\}_n P_g^{-\frac{1}{2}} \le I$$

Consequently, we can derive the following inequality

$$\max_{t>0}|\{z_2(t)\}_n|^2 \le \max_{t>0}||x^T(t)\{C_2\}_n^T\{C_2\}_n x(t)||_2 \le I, \tag{26}$$

which implies that (24) is held, thereby ensuring indices (ii) and (iii) in Table 1. This completes the proof. □

Theorem 2. *Given the positive scalars $\eta_M, \bar{\alpha}, \hat{\alpha}\kappa, \sigma, \varepsilon$ and δ_i, λ_m with $i \in \{1,2\}, m \in \{1,2,3\}$, the system (10) is MSAS and satisfies H_∞ performance indices in Table 1, if there exist matrices $X > 0, \tilde{Q} > 0, \tilde{R} > 0, \tilde{M} > 0$ and $\tilde{\Phi} > 0$ such that*

$$\tilde{\Psi} = \begin{bmatrix} \tilde{\Theta} & * & * \\ \tilde{C} & -I & * \\ \tilde{D} & 0 & -X \end{bmatrix} < 0, \tag{27}$$

$$\begin{bmatrix} -I & * \\ \sqrt{\nu}X\{C_2\}_n^T & -X \end{bmatrix} < 0, \ (n = 1,2) \tag{28}$$

$$\tilde{\mathcal{R}} = \begin{bmatrix} \tilde{\hat{R}} & * \\ \tilde{H}^T & \tilde{\hat{R}} \end{bmatrix} > 0, \tag{29}$$

where

$$\tilde{\Theta} = \begin{bmatrix} \tilde{\Psi}_1 & * & * \\ \eta_M\tilde{\mathcal{A}} & \Xi & * \\ \eta_M\tilde{\mathcal{B}} & 0 & \Xi \end{bmatrix}, \tilde{\Psi} = \tilde{\Psi}_1, \tilde{\Psi}_1 = [\tilde{\Pi}]_{12\times 12},$$

$$\tilde{\Pi}_{11} = XA^T + AX + \tilde{Q} - 4\tilde{R},$$

$$\tilde{\Pi}_{21} = \sum_{m=1}^{3}(1-\bar{\alpha})(Y_m^T B^T) - 2\tilde{R} - \tilde{H}_1^T - \tilde{H}_2 - \tilde{H}_2^T - \tilde{H}_3^T,$$

$$\tilde{\Pi}_{22} = \mu_1\tilde{\Phi} - 8\tilde{R} + \tilde{H}_1^T + \tilde{H}_1 - \tilde{H}_3^T - \tilde{H}_3,$$

$$\tilde{\Pi}_{31} = \tilde{H}_1^T - \tilde{H}_2 + \tilde{H}_2^T - \tilde{H}_3^T, \tilde{\Pi}_{33} = -\tilde{Q} - 4\tilde{R},$$

$$\tilde{\Pi}_{32} = -2\tilde{R} - \tilde{H}_1^T + \tilde{H}_2 + \tilde{H}_2^T - \tilde{H}_3^T,$$

$$\tilde{\Pi}_{(m+3)1} = 2(1-\bar{\alpha})Y_m^T B^T, \tilde{\Pi}_{(m+3)2} = \frac{2}{3}\mu_1\tilde{\Phi},$$

$$\tilde{\Pi}_{44} = \left(-\mu_{31} + \frac{4}{9}\mu_1\right)\tilde{\Phi}, \tilde{\Pi}_{54} = \left(\frac{4}{9}\mu_1 + \mu_2\right)\tilde{\Phi},$$

$$\tilde{\Pi}_{55} = \left(-\mu_{32} + \frac{4}{9}\mu_1 - 2\mu_2\right)\tilde{\Phi}, \tilde{\Pi}_{64} = \left(\frac{4}{9}\mu_1 - \mu_2\right)\sigma_4\tilde{\Phi},$$

$$\tilde{\Pi}_{65} = \left(\frac{4}{9}\mu_1 + \mu_2\right)\tilde{\Phi}, \tilde{\Pi}_{66} = \left(-\mu_{33} + \frac{4}{9}\mu_1\right)\tilde{\Phi}, \tilde{\Pi}_{71} = 6\tilde{R},$$

$$\tilde{\Pi}_{72} = 6\tilde{R} + 2\tilde{H}_2 + 2\tilde{H}_3, \tilde{\Pi}_{73} = -2\tilde{H}_2 + 2\tilde{H}_3,$$

$$\tilde{\Pi}_{77} = \tilde{\Pi}_{88} = -12\tilde{R}, \tilde{\Pi}_{81} = 2\tilde{H}_2 + \tilde{H}_3^T,$$

$$\tilde{\Pi}_{82} = 6\tilde{R} - 2\tilde{H}_2 + 2\tilde{H}_3^T, \tilde{\Pi}_{83} = 6\tilde{R}, \tilde{\Pi}_{87} = -4\tilde{H}_3^T,$$

$$\tilde{\Pi}_{(m+8)1} = \bar{\alpha}Y_m^T B^T, \tilde{\Pi}_{(m+8)(m+8)} = -P, \tilde{\Pi}_{121} = D^T P,$$

$$\tilde{\Pi}_{1212} = -\gamma^2 I, \Xi = \varepsilon^2\tilde{R} - 2\varepsilon X,$$

$$\tilde{\mathcal{A}} = \begin{bmatrix} AX & (1-\bar{\alpha})\tilde{\mathscr{B}}_1 & 0 & 2(1-\bar{\alpha})\tilde{\mathscr{B}}_2 & 0 & 0 & \bar{\alpha}\tilde{\mathscr{B}}_2 & D \end{bmatrix},$$

$$\tilde{\mathcal{B}} = \begin{bmatrix} 0 & \hat{\alpha}\tilde{\mathscr{B}}_1 & 0 & 2\hat{\alpha}\tilde{\mathscr{B}}_2 & 0 & 0 & \hat{\alpha}\tilde{\mathscr{B}}_2 & 0 \end{bmatrix},$$

$$\tilde{\mathcal{C}} = \begin{bmatrix} C_1 & (1-\bar{\alpha})\tilde{\mathscr{D}}_1 & 0 & 2(1-\bar{\alpha})\tilde{\mathscr{D}}_2 & 0 & 0 & \bar{\alpha}\tilde{\mathscr{D}}_2 & 0 \end{bmatrix},$$

$$D = \begin{bmatrix} \sqrt{3}LX & \underbrace{0 \ \dots \ 0}_{11} \end{bmatrix}, \tilde{\hat{R}} = \begin{bmatrix} \tilde{R} & 0 \\ 0 & 3\tilde{R} \end{bmatrix}, \tilde{H} = \begin{bmatrix} \tilde{H}_1 & * \\ \tilde{H}_2 & \tilde{H}_3 \end{bmatrix},$$

$$\tilde{\mathscr{B}}_1 = \sum_{m=1}^{3} BY_m, \tilde{\mathscr{B}}_2 = \begin{bmatrix} BY_1 & BY_2 & BY_3 \end{bmatrix},$$

$$\tilde{\mathscr{D}}_1 = \sum_{m=1}^{3} D_1 Y_m, \tilde{\mathscr{D}}_2 = \begin{bmatrix} D_1Y_1 & D_1Y_2 & D_1Y_3 \end{bmatrix}.$$

Furthermore, the designed controller feedback gain and triggering matrix can be computed by $K_m = Y_m X^{-1}$, $\Phi = X^{-1}\tilde{\Phi}X^{-1}$.

Proof. Consider the following definitions:

$$\chi = diag\left\{\underbrace{X, \dots, X}_{11}, \underbrace{I, \dots, I}_{5}\right\}, \tilde{H} = \begin{bmatrix} \tilde{H}_1 & * \\ \tilde{H}_2 & \tilde{H}_3 \end{bmatrix},$$

$$\tilde{H}_1 = XH_1X, \tilde{H}_2 = XH_2^TX, \tilde{H}_3 = XH_3^TX, \tilde{R} = XRX,$$

$$\tilde{Q} = XQX, Y_m = K_mX, \tilde{\Phi} = X\Phi X, X = P^{-1}.$$

Using Schur complement [37] to (11), one can obtain that

$$\begin{bmatrix} \Theta & * & * \\ C & -I & * \\ D & 0 & -P^{-1} \end{bmatrix} < 0 \tag{30}$$

where $\Theta = \begin{bmatrix} \Psi_1 & * & * \\ \eta_M\mathcal{A} & -R^{-1} & * \\ \eta_M\mathcal{B} & 0 & -R^{-1} \end{bmatrix}$.

Note that $R^{-1} \le -2\varepsilon X + \varepsilon^2\tilde{R}$, then we can conclude that (27) serves as a sufficient condition to ensure the validity of (30) by both left- and right-multiplying (30) with the matrix χ. Following the similar operation, one can derive (28) and (29). The proof is completed. □

4. Simulation example

The effectiveness of the proposed approach is demonstrated in this section. Fig. 1 depicts the structure of a QVSS, with its dynamics described by (1). Based on the full-vehicle suspension system model of a

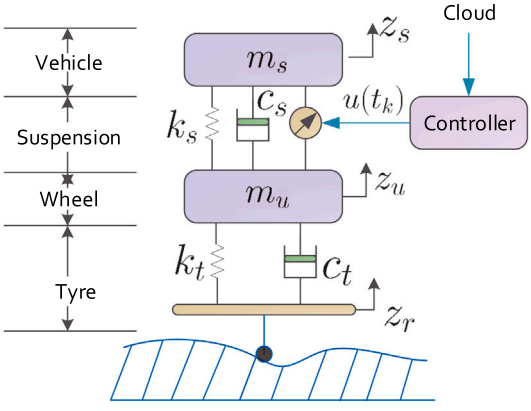

Fig. 1. Structure of a QVSS.

Table 2
QVSS model parameter.

Terminologies	Value	Terminologies	Value
m_s (kg)	350	m_u (kg)	100
k_s (kN/m)	30	k_t (kN/m)	200
c_s (kNs/m)	1.2	c_t (Ns/m)	160

D-class vehicle and commonly used parameters for a simplified QVSS in [4,7], the relevant parameters are listed in Table 2.

Choose $h = 0.01\ s$, $\gamma = 30$, $\delta_1 = 0.01, \delta_2 = 0.1, \sigma = 0.1, \lambda_1 = 0.5, \lambda_2 = 0.3, \lambda_3 = 0.2, \varepsilon = 0.9, \beta_0 = 1$, $\eta_M = 0.07, \bar{\alpha} = 0.1, \hat{\alpha} = 0.3$, $z_{max} = 0.03$. Assume the deception attacks $\aleph(t) = \left[-\tanh(0.35x_1(t)), -\tanh(0.3x_2(t)), -\tanh(0.25x_3(t)), -\tanh(0.45x_4(t))\right]$, and $L = \mathrm{diag}\{0.35, 0.3, 0.25, 0.45\}$.

Similar to previous works [15], we employ the road profile $z_r(t)$ to replicate varied road conditions with different frequencies for the QVSS.

$$z_r(t) = 0.02\sin 2\pi t + 0.001\sin 10\pi t + 0.001\sin 16\pi t. \tag{31}$$

From Theorem 2, the parameter matrix Φ, K_1,K_2, and K_3 can be derived as

$$\Phi = 10^4 \times \begin{bmatrix} 1.4972 & 0.2282 & -0.1235 & 0.0170 \\ 0.2282 & 8.4446 & -0.4465 & 0.0266 \\ -0.1235 & -0.4465 & 0.1821 & -0.0023 \\ 0.0170 & 0.0266 & -0.0023 & 0.0043 \end{bmatrix},$$

$$K_1 = \begin{bmatrix} 189.4800 & 882.8504 & -275.1329 & -5.3820 \end{bmatrix},$$

$$K_2 = \begin{bmatrix} 98.3761 & 495.2638 & -150.6537 & -3.4445 \end{bmatrix},$$

$$K_3 = \begin{bmatrix} 89.3595 & 381.4276 & -122.3645 & -1.9238 \end{bmatrix}.$$

Figs. 2–4 represent the responses of the QVSS, where the blue solid lines represent the body acceleration, suspension deflection, and tire deflection—corresponding to ride comfort, suspension stroke, and road holding in Table 1—under the influence of the road profile (31), and the passive SSs are represented by the red dashed lines. These figures demonstrate that the performance indices in Table 1 are effectively maintained at satisfactory levels, even in the presence of random deception attacks.

Furthermore, the release intervals in Fig. 5 demonstrate that the proposed ETM discards a significant number of data packets, highlighting its efficiency in resource optimization. The incorporation of past

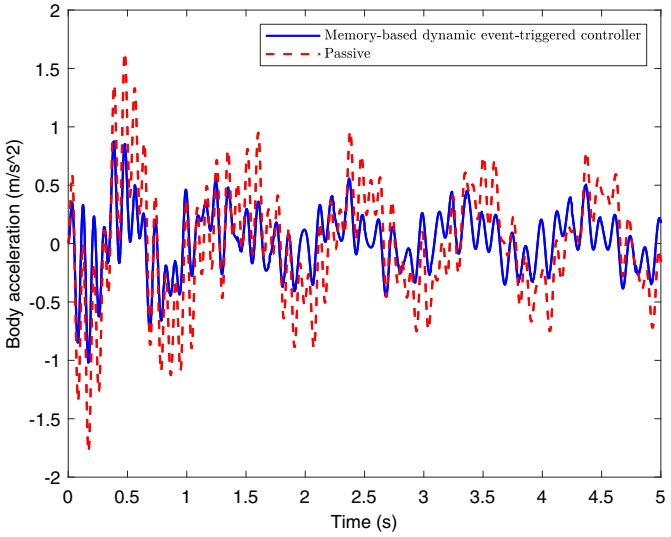

Fig. 2. Body acceleration.

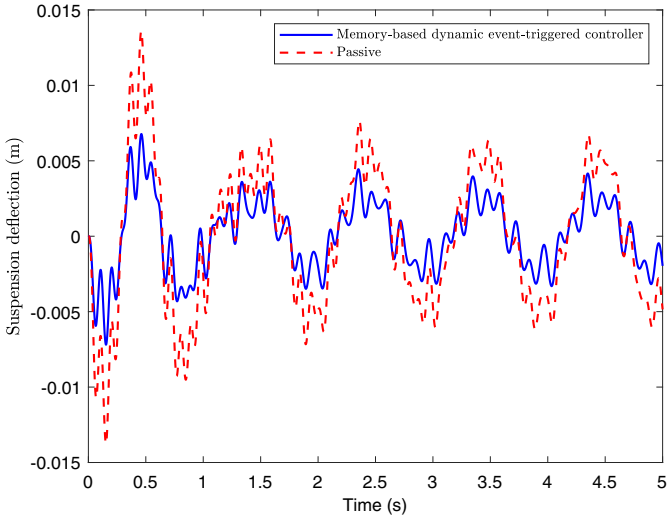

Fig. 3. Suspension deflection.

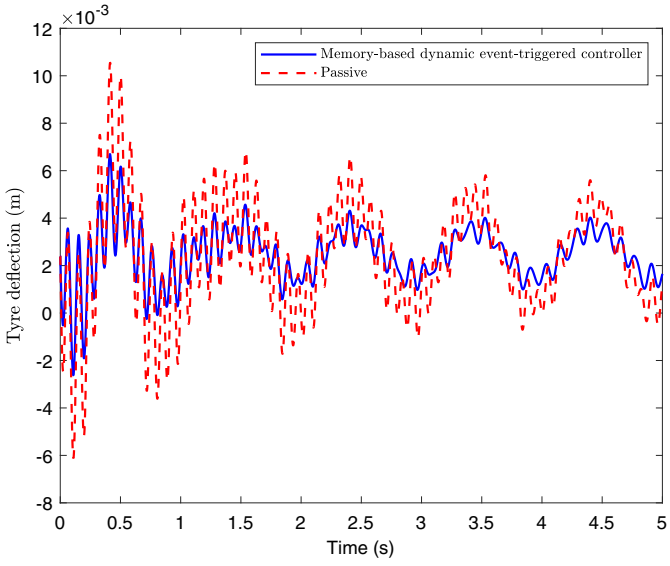

Fig. 4. Tire deflection.

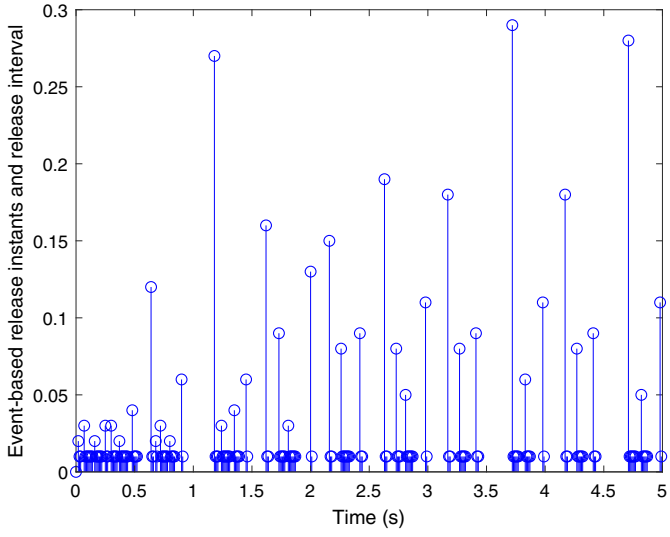

Fig. 5. Releasing intervals under memory-based dynamic ETM

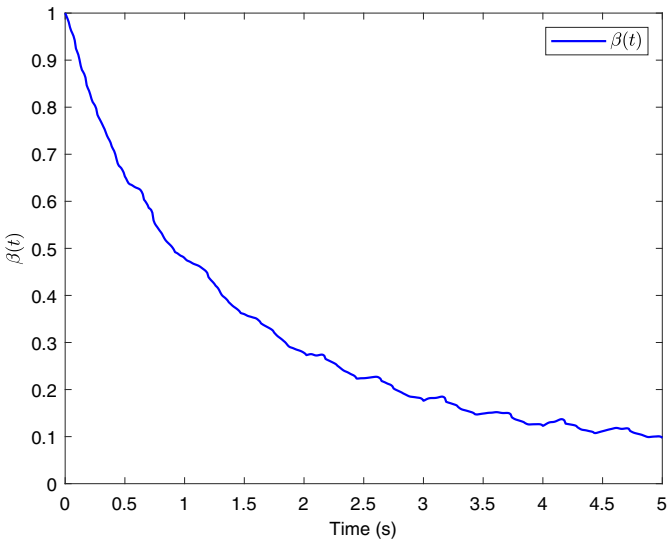

Fig. 6. Dynamic variable $\beta(t)$.

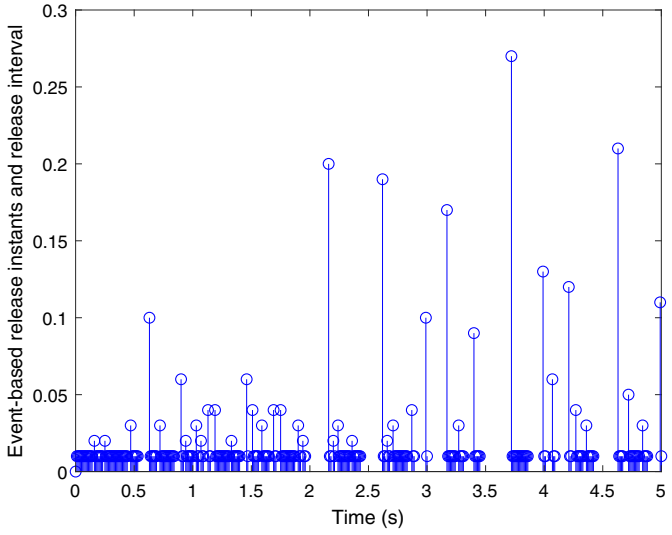

Fig. 7. Releasing intervals under the memory-based ETM in [26].

release information as input in the ETM is crucial in reducing false-triggered events by leveraging average information. Additionally, the dynamic variable in the triggering laws, shown in Fig. 6, is continuously adjusted over time, enabling adaptive scheduling of network data transmission. This strategy effectively optimizes the data transmission workload, enhancing overall system performance.

By choosing $\beta_0 = 0$, $\sigma = 0$, and $\delta_2 = 0$, the proposed DMETM will reduce to be an memory-based ETM in [26]. Keeping all other parameters unchanged, by Theorem 2, the parameter matrix Φ, K_1,K_2, and K_3 can be derived as:

$$\Phi = 10^4 \times \begin{bmatrix} 1.6188 & 0.2277 & -0.1376 & 0.0187 \\ 0.2277 & 9.2593 & -0.4950 & 0.0291 \\ -0.1376 & -0.4950 & 0.2013 & -0.0025 \\ 0.0187 & 0.0291 & -0.0025 & 0.0047 \end{bmatrix},$$

$$K_1 = \begin{bmatrix} 181.5457 & 868.2795 & -268.7001 & -5.5009 \end{bmatrix},$$

$$K_2 = \begin{bmatrix} 105.4707 & 513.2914 & -157.9605 & -3.3516 \end{bmatrix},$$

$$K_3 = \begin{bmatrix} 88.7311 & 380.9043 & -122.1391 & -1.9263 \end{bmatrix}.$$

Fig. 7 illustrates the release intervals of QVSSs under the memory-based ETM in [26]. To clarify the role of the designed dynamic variables in (3), the data release rate (DDR) is formally defined as DDR = released data packets/sampled data packets. Statistical analysis reveals that the DDR for DMETM is 35.8 %, whereas the memory-based ETM exhibits a DDR of 54.8 %. A comparative analysis indicates that the continuous fine-tuning of dynamic variables within the triggering rules significantly enhances the dynamic scheduling of network data transmission. This approach not only ensures optimal system performance but also conserves substantial network bandwidth.

5. Conclusion

This paper introduces an innovative memory-based dynamic ETM to effectively address the challenge of ensuring both driving safety and comfort in active QVSSs under deception attacks. To reduce the data transmission workload and optimize transmitted information, a memory-based dynamic ETM is proposed. Additionally, the asymptotic stability in mean-square sense and H_∞ index of the system are analyzed using the Lyapunov–Krasovskii function method. The proposed memory-based dynamic ETM not only minimizes false-triggered events by leveraging average information but also enables dynamic scheduling of network data transmission through the continuous adjustment of dynamic variables in the triggering laws. Simulation results validate the effectiveness of the proposed control protocol in enhancing both driving comfort and safety. Future work will focus on optimizing the ETM for suspension systems by integrating the latest results with approaches such as those in [38], aiming to develop more flexible and efficient ETMs.

CRediT authorship contribution statement

Wangrui Cheng: Writing – review & editing, Validation, Methodology, Formal analysis. **Tingting Yin:** Writing – original draft, Methodology. **Zhou Gu:** Methodology, Funding acquisition.

Declaration of competing interest

The authors declare that they have no known competing financial interests or personal relationships that could have appeared to influence the work reported in this paper.

References

[1] Shah D, Mauro SMM, Chaoui H, Tusto JF. Event-triggered non-switching networked sliding mode control for active suspension system with random actuation network delay. IEEE Trans Intell Transp Syst 2022; 23(7):7521–34.
[2] Hu MJ, Park JH, Cheng J. Robust fuzzy delayed sampled-data control for nonlinear active suspension systems with varying vehicle load and frequency-domain constraint. Nonlinear Dyn 2021;105(3):2265–81.
[3] Liu L, Zhu C, Liu YJ, Tong S. Intelligent motion tracking control of vehicle suspension systems with constraints via neural performance analysis. IEEE Trans Intell Transp Syst 2022;23(8):13896–903.
[4] Ge X, Ahmad I, Han QL, Wang J, Zhang XM. Dynamic event-triggered scheduling and control for vehicle active suspension over controller area network. Mech Syst Signal Process 2021;152:107481.
[5] Yatak M, Sahin F. Ride comfort-road holding trade-off improvement of full vehicle active suspension system by interval type-2 fuzzy control. Eng Sci Technol Int J 2021;24(1):259–70.
[6] Li Z, Zheng L, Ren Y, Li Y, Xiong Z. Multi-objective optimization of active suspension system in electric vehicle with in-wheel-motor against the negative electromechanical coupling effects. Mech Syst Signal Process 2019;116:545–65.
[7] Li H, Liu H, Gao H, Shi P. Reliable fuzzy control for active suspension systems with actuator delay and fault. IEEE Trans Fuzzy Syst 2012;20(2):342–57.
[8] Li H, Jing X, Lam HK, Shi P. Fuzzy sampled-data control for uncertain vehicle suspension systems. IEEE Trans Cybernet 2014;44(7):1111–26.
[9] Wang T, Wu J, Wang Y, Ma M. Adaptive fuzzy tracking control for a class of strict-feedback nonlinear systems with time-varying input delay and full state constraints. IEEE Trans Fuzzy Syst 2020;28(12):3432–41.
[10] Wen S, Chen MZQ, Zeng Z, Yu X, Huang T. Fuzzy control for uncertain vehicle active suspension systems via dynamic sliding-mode approach. IEEE Trans Syst Man Cybern Syst 2017;47(1):24–32.

[11] Zhang M, Jing X. A bioinspired dynamics-based adaptive fuzzy SMC method for half-car active suspension systems with input dead zones and saturations. IEEE Trans Cybern 2021;51(4):1743–55.
[12] Sun W, Gao H, Kaynak O. Adaptive backstepping control for active suspension systems with hard constraints. IEEE/ASME Trans Mechatronics 2013;18(3):1072–79.
[13] Zheng X, Zhang H, Yan H, Yang F, Wang Z, Vlacic L. Active full-vehicle suspension control via cloud-aided adaptive backstepping approach. IEEE Trans Cybern 2020;50(7):3113–24.
[14] Li W, Du H, Feng Z, Deng L, Ning D, Li W. Stability analysis for H-infinity-controlled active quarter-vehicle suspension systems with a resilient event-triggered scheme under periodic DoS attacks. IEEE Trans Cybern 2024;54(4):2358–68.
[15] Gu Z, Sun X, Lam HK, Yue D, Xie X. Event-based secure control of T-S fuzzy based 5-DOF active semi-vehicle suspension systems subject to DoS attacks. IEEE Trans Fuzzy Syst 2022;30(6):2032–43.
[16] Zhu W, Jiang ZP. Event-based leader-following consensus of multi-agent systems with input time delay. IEEE Trans Autom Control 2015;60(5):1362–67.
[17] Gu Z, Yan S, Ahn CK, Yue D, Xie X. Event-triggered dissipative tracking control of networked control systems with distributed communication delay. IEEE Syst J 2022;16(2):3320–30.
[18] Yang D, Ren W, Liu X, Chen W. Decentralized event-triggered consensus for linear multi-agent systems under general directed graphs. Automatica 2016;69:242–49.
[19] Ma B, Lu Q, Gu Z. Resilient event-based fuzzy fault detection for DC microgrids in finite-frequency domain against DoS attacks. Sensors 2024;24(9):2677.
[20] Gu Z, Yue D, Park JH, Xie X, Memory-event-triggered fault detection of networked IT2 T-S fuzzy systems. IEEE Trans Cybern 2023;53(2):743–52.
[21] Yue D, Tian E, Han QL. A delay system method for designing event-triggered controllers of networked control systems. IEEE Trans Autom Control 2013;58(2):475–81.
[22] Fu J, Qi Y, Xing N, Li Y. A new switching law for event-triggered switched systems under DoS attacks. Automatica 2022;142:110373.
[23] Fei Z, Wang X, Liu M, Yu J. Reliable control for vehicle active suspension systems under event-triggered scheme with frequency range limitation. IEEE Trans Syst Man Cybern Syst 2021;51(3):1630–41.
[24] Jia T, Pan Y, Liang H, Lam HK. Event-based adaptive fixed-time fuzzy control for active vehicle suspension systems with time-varying displacement constraint. IEEE Trans Fuzzy Syst 2022;30(8):2813–21.
[25] Gu Z, Huang X, Sun X, Xie X, Park JH, Memory-event-triggered tracking control for intelligent vehicle transportation systems: a leader-following approach, IEEE Trans Intell Transp Syst, 2024;25(5):743–52.
[26] Tian E, Peng C. Memory-based event-triggering H_∞ load frequency control for power systems under deception attacks. IEEE Trans Cybern 2020;50(11):4610–18.
[27] Li X, Sun Z, Tang Y, Karimi HR. Adaptive event-triggered consensus of Multiagent systems on directed graphs. IEEE Trans Autom Control 2021;66(4):1670–85.
[28] Girard A. Dynamic triggering mechanisms for event-triggered control. IEEE Trans Autom Control 2015;60(7):1992–97.
[29] Lv X, Niu Y, Park JH, Song J. Sliding mode control for 2D FMII systems: A bidirectional dynamic event-triggered strategy. Automatica 2023;147:110727.
[30] Ye D, Zhang TY. Summation detector for false data-injection attack in cyber-physical systems. IEEE Trans Cybern 2020;50(6):2338–45.
[31] Zhang XM, Han QL, Ge X, Ding L. Resilient control design based on a sampled-data model for a class of networked control systems under denial-of-service attacks. IEEE Trans Cybern 2020;50(8):3616–26.
[32] Ge X, Han QL, Zhong M, Zhang XM. Distributed krein space-based attack detection over sensor networks under deception attacks. Automatica 2020;109:108557.
[33] Ding D, Wang Z, Han QL, Wei G. Security control for discrete time stochastic nonlinear systems subject to deception attacks. IEEE Trans Syst Man Cybern Syst 2018;48(5):779–89.
[34] Gao X, Deng F, Su CY, Zeng P. Protocol-based fuzzy control of networked systems under joint deception attacks. IEEE Trans Fuzzy Syst 2022;31(3):1052–63.
[35] Seuret A, Gouaisbaut F. Wirtinger-based integral inequality: application to time-delay systems. Automatica 2013;49(9):2860–66.
[36] Seuret A, Gouaisbaut F, Fridman E. Stability of systems with fast-varying delay using improved Wirtinger's inequality. In: Proc. 52nd IEEE conf decis control. Florence; 2013. p. 946–51.
[37] Cao J, Yuan K, Li HX. Global asymptotical stability of recurrent neural networks with multiple discrete delays and distributed delays. IEEE Trans Neural Netw 2006;17(6):1646–51.
[38] Gu Z, Fan Y, Yin T, Yan S, A novel event-triggered load frequency control for power systems with electric vehicle integration, IEEE Trans Syst Man Cybern Syst 2025;55(1):599–608.